



Article

Ablation Mechanism of AlSiB-C/C Composites under an Oxy-Acetylene Torch

Qiuchen Han ¹, Lei Chang ¹, Zhaoqun Sun ², Jiaqi Sun ¹, Zengyan Wei ^{1,*} , Pingping Wang ^{1,*}, Ziyang Xiu ¹, Huasong Gou ¹, Pengchao Kang ^{1,*}  and Gaohui Wu ¹

¹ School of Materials Science and Engineering, Harbin Institute of Technology, Harbin 150001, China

² Laboratory No. 8, Institute of Electronic System Engineering, Beijing 100854, China

* Correspondence: zwei@hit.edu.cn (Z.W.); hit_wangpingping@163.com (P.W.); kangpc@hit.edu.cn (P.K.)

Abstract: In order to improve the ablation resistance of C/C composites, an AlSiB alloy (mass ratio of Al/Si/B = 2:4:1) was used as a dissipative agent to fill the pores of a C/C composites matrix by reactive melt infiltration to prepare AlSiB-C/C composites. The microstructure evolution and ablation behavior of the obtained AlSiB-C/C composites (mass ratio of Al/Si/B = 2:4:1) under oxy-acetylene flame were investigated by SEM after ablating for 25 s, 50 s, 100 s and 150 s. At the beginning of the ablation process, thermal chemical erosion played a leading part. By using the heat-absorption effect of sweating and the sealing protection effect of the oxide layer, AlSiB-C/C composites significantly reduced the ablation surface temperature, and the linear ablation rate was 4.04 $\mu\text{m/s}$. With the process of ablation, thermal mechanical erosion tended to dominate. The specimen surface could not form a continuous covering of oxide film to slow down the flame scour, resulting in non-uniform ablation and further expansion of the ablation pit. The self-transpiration cooling behavior and the self-sealing of the ablation products of the dissipative agent played an important role in reducing the extent of thermal chemical erosion and preventing matrix ablation.

Keywords: reactive melt infiltration; ablation resistance; AlSiB-C/C composites; oxy-acetylene flame; heat dissipation



Citation: Han, Q.; Chang, L.; Sun, Z.; Sun, J.; Wei, Z.; Wang, P.; Xiu, Z.; Gou, H.; Kang, P.; Wu, G. Ablation Mechanism of AlSiB-C/C Composites under an Oxy-Acetylene Torch. *Metals* **2023**, *13*, 160. <https://doi.org/10.3390/met13010160>

Academic Editor: Manoj Gupta

Received: 27 November 2022

Revised: 21 December 2022

Accepted: 9 January 2023

Published: 12 January 2023



Copyright: © 2023 by the authors. Licensee MDPI, Basel, Switzerland. This article is an open access article distributed under the terms and conditions of the Creative Commons Attribution (CC BY) license (<https://creativecommons.org/licenses/by/4.0/>).

1. Introduction

The carbon/carbon (C/C) composites have a series of special properties, such as a low density ($<2.0 \text{ g/cm}^3$), a low coefficient of thermal expansion ($1\text{--}2 \times 10^{-6} \text{ /K}$), a high specific strength/modulus ($\sim 20 \text{ GPa}$) and thermal shock resistance [1–3]. They have been used in the missile re-entry thermal protection system, solid rocket motor nozzles and aircraft braking systems [4]. Unfortunately, carbon materials are apt to be oxidized above 400°C in an atmospheric environment, which restricts their applications in high-temperature and oxygen-containing environments [5]. Previous research has mainly focused on introducing SiC [6], ZrC [7], ZrB_2 [8], HfC [9], TaC [10] and other ultrahigh temperature ceramics into the carbon matrix in order to improve the oxidation resistance and ablation resistance of C/C composites. The excellent oxidation resistance of ultrahigh temperature ceramics is closely related to its oxidation products. Zou et al. [11] found that the addition of silica-scale formers, such as SiC, could improve the ablation resistance of ZrB_2 due to the formation of a borosilicate glass that could act as a barrier to oxygen diffusion. Yang et al. [12] prepared C/C-HfC-ZrC-SiC, whose ablation rates is one order of magnitude lower than that of C/C-HfC composites. The melting point of ZrO_2 and HfO_2 are about 2700°C , which can resist extremely high heat flux. These studies show that the thermochemical ablation rate is mainly controlled by temperature and oxidation reactions. Therefore, reducing the ablation temperature and hindering the diffusion of oxygen into the carbon matrix can effectively improve the ablation resistance. Using the huge latent heat of phase change materials to reduce the heat load of ablated surfaces has been confirmed to be a promising

thermal protection method. Researchers have developed W/Cu (17.4 g/cm^3), C/C-Cu (2.9 g/cm^3) and TiB_2/Cu (5.43 g/cm^3) composites, which can be applied to transpiration cooling systems [13–15]. However, copper matrix composites have the disadvantages of high density and a high thermal expansion coefficient ($>5.6 \times 10^{-6}/\text{K}$), which will lead to thermal failure and structural failure. Aluminum alloy has a low melting point ($<660^\circ\text{C}$), a high melting latent heat (10.67 kJ/mol), a high boiling point ($\sim 2460^\circ\text{C}$) and low vapor pressure (0.13 kPa , 1284°C) [16]. Our group has recently developed a variety of dissipative and heat-resistant composites, such as Al/graphite [17], Al₂₀Si/graphite [18] and Si₂₀Mo/graphite [19], which form self-healing protective films (Al_2O_3 , SiO_2 , etc.) while reducing the surface temperature. The aluminum in these composites can be used to remove partial heat from the components subject to high heat loads through transpiration cooling mechanisms. For instance, the temperature difference between the graphite and the AlSi/graphite composite has been reported to be approximately 300°C in the literature [18]. Other researchers have used similar principles in order to significantly improve the ablation resistance. Tian et al. [20] designed an intelligent cooling structure using “z-pin” silicon rods. After ablating for 300 s, the surface temperature was approximately 200°C lower than the sample without “Z-pins like” Si rods, and the linear ablation rates of the sample were 112.72% lower than the sample without “Z-pins like” Si rods. Although many investigations have been carried out on graphite matrix composites, C/C matrix composites by reactive infiltration are seldom reported. In order to further expand the application of C/C composites, our research focused on developing composites with excellent ablation resistance through a low cost and simple method. In this paper, AlSiB-C/C composites were prepared by reactive infiltration using the idea of phase change cooling and self-oxidation protection. The surface morphology evolution and ablation mechanism under an oxy-acetylene flame were investigated.

2. Materials and Methods

The C/C composites (supplied by Jilin Carbon Co., Ltd., Jilin, China) and high pure Al (200 μm , 99.5%), Si (1 mm, 99.9%) and B (1 mm, 99.9%) powders (supplied by Beijing Xingrongyuan Science & Technology Co., Ltd., Beijing China) were used as raw materials in order to prepare the AlSiB-C/C composites in the present work. The C/C composites were fabricated from a three-dimensional (3D) carbon fiber preform with an open porosity of 23.58%. 3D needle-punched carbon fiber (T700, 6K) reinforcements were prepared using a needling method in a $100 \text{ mm} \times 30 \text{ mm} \times 20 \text{ mm}$ space. The morphology and pore-size distribution of the C/C composites are shown in Figure 1, and the relevant properties of the C/C composites are listed in Table 1. The C/C composites contained several irregularly shaped pores (Figure 1a), and their corresponding diameters ranged from 10 to $20 \mu\text{m}$ (Figure 1b).

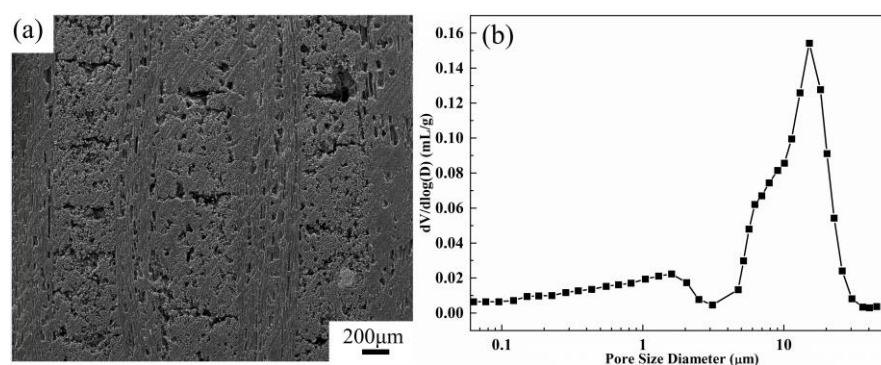


Figure 1. SEM image (a) and pore-size distribution (b) of the C/C composites.

Table 1. Properties of the C/C composites.

Volume density (g/cm ³)	1.63
Porosity (vol%)	23.58
Most probable aperture (μm)	17.71
Mean aperture (μm)	0.11

The AlSiB-C/C composites were prepared by reactive melt infiltration. The composition of the AlSiB alloy was as follows: Al:Si:B = 2:4:1 (Mass percentage). The AlSiB alloy powder was mixed by low-speed ball-milling at 50 rpm for 10 h. Figure 2 shows a schematic diagram of the device for infiltrating the AlSiB alloy. Before infiltration, the porous C/C composites, which were fixed on the lifting device in advance by a high-density graphite rod to form a preform, were placed in a graphite crucible in a vacuum furnace together with Al-Si-B mixed powder (Figure 2a). The furnace was heated to 1600 °C by 50 °C/min in a vacuum atmosphere. Then, a pressure of 0.1 MPa was applied under argon for 5 min in order to promote the infiltration of Al, Si and B into the C/C composites (Figure 2b). Afterwards, the infiltrated C/C composites were pulled out from the molten alloy by the lifting device and cooled to room temperature, and then the AlSiB-C/C composites were obtained (Figure 2c).

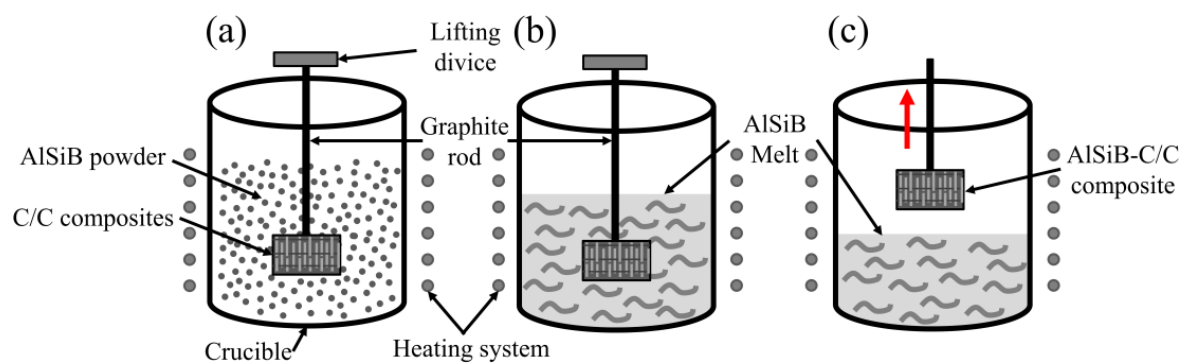


Figure 2. Schematic diagram of the device for infiltrating the AlSiB alloy. (a) embedded into powders; (b) Reactive melt infiltration; (c) Pull out the sample after infiltration.

The specimens (3 mm × 4 mm × 40 mm) were obtained by wire-electrode cutting in order to investigate the three-point bending strength using a WDW-100 electronic universal testing machine. The ablation behavior was tested in a flowing oxy-acetylene flame environment. The rate of flow and pressure of oxygen and acetylene were 1512 L/h and 0.4 MPa, and 1116 L/h and 0.095 MPa, respectively. The distance between the nozzle tip and the surface of the specimens was 10 mm, and the inner diameter of the nozzle tip was 2.0 mm. During the test, the specimens, with a size of Φ30 × 10 mm, were exposed to the flame. The ablation angle was 90°. The heat flux was 4186.8 ± 418.68 kW/m², and the temperature of the oxy-acetylene flame measured by an optical pyrometer was 2700–3000 °C. The specimens, fixed in a graphite concave, were exposed to the flame for different durations (25 s, 50 s, 100 s and 150 s). The temperature of the ablation surface was measured using an optical pyrometer (Raytek MR1SCSF, Santa Cruz, CA, USA)). The linear ablation rate (LAR) and mass ablation rate (MAR) were evaluated according to the following equation [21]:

$$R_l = \frac{l_0 - l_1}{\Delta t} \quad (1)$$

$$R_m = \frac{m_0 - m_1}{\Delta t} \quad (2)$$

where R_l and R_m are the linear and mass ablation rates, respectively, l_0 and l_1 are the thickness of the specimens before and after ablation, respectively, m_0 and m_1 are the mass of the specimens before and after ablation, respectively, and Δt is the ablation time [21].

The morphologies and chemical compositions of the prepared composites before and after ablation were investigated using a scanning electron microscope (SEM, Quanta 200FEG, FEI Inc, Holland equipped with energy dispersive spectroscopy (EDS). The phase analysis of the prepared composites before and after ablation were conducted using X-ray diffraction (XRD, X'Pert Pro MPD, Panalytical B.V., Almelo, The Netherlands) with a Cu K α radiation ($\lambda = 0.1542$ nm). The diffraction angle range was between 20° and 90°, with a step width of 0.033°. The thermal diffusivity was measured using a LFA447 laser thermal conductivity meter (Netsch, Selb Germany). The specimen size was $\Phi 12.7 \times 3$ mm, and the temperature measurement range was between 25 °C and 300 °C with a heating rate of 2 °C/min. The porosity and bulk density of the specimens were measured using the Archimedes method with distilled water at room temperature.

3. Results and Discussion

3.1. Microstructure of AlSiB-C/C Composites

Figure 3 shows the SEM images of the cross-section and the corresponding EDS analyses of the AlSiB-C/C composites. It is clear that the former pores in the C/C preform have been filled with AlSiB alloy (Figure 3a). The density of the AlSiB-C/C composites was 2.10 g/cm³ and the porosity was calculated to be 4.52%. Figure 4 shows the flexural strength of the obtained AlSiB-C/C composites and C/C composites with five specimens per test. The flexural strength of the AlSiB-C/C composites was 162.65 MPa, which was 34.96% higher than the 120.52 MPa of the C/C composites.

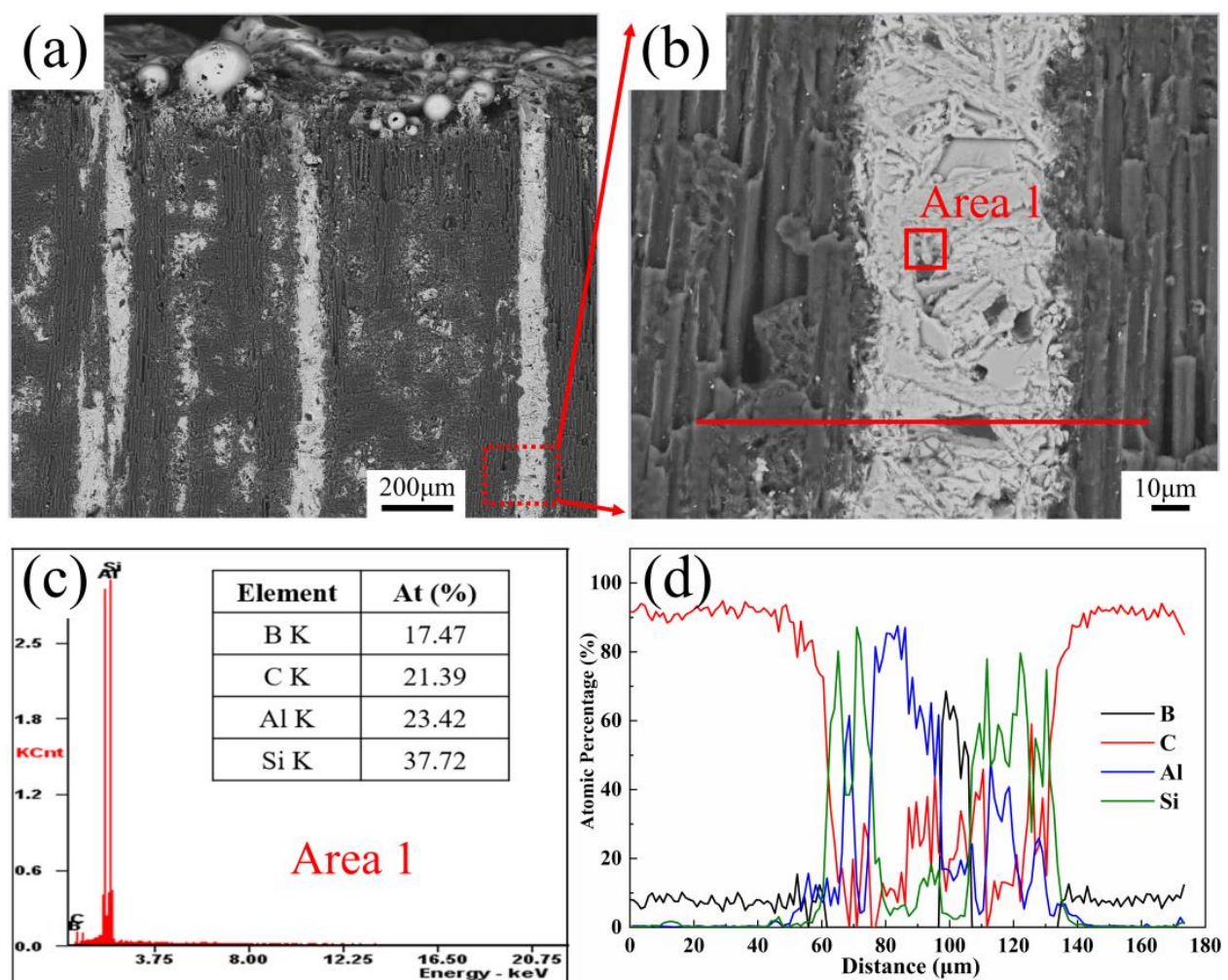


Figure 3. SEM image of the AlSiB-C/C composites (a,b), and the EDS analysis results (c,d) of Area 1 and the red line, respectively.

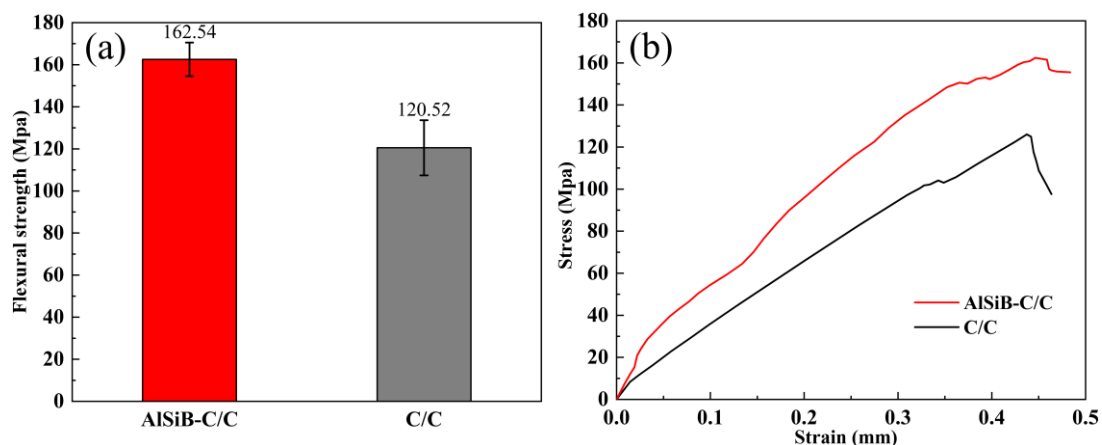


Figure 4. (a) Flexural strength and (b) the stress–strain curve of AlSiB-C/C and C/C.

The high magnification image (Figure 3b) revealed the presence of two regions that were distinguished by different colors, where dark areas indicated the carbon fiber preform and bright areas indicated the AlSiB alloy. The distribution of the AlSiB alloy is consistent with the length direction of the carbon fibers because there are more connected pores in the carbon fibers distributed in parallel. The EDS analysis of Area 1 and the profile analysis along the red line are shown in Figure 3c,d, respectively. It has been revealed that Area 1 was mainly composed of 17.47 at.% B, 21.9 at.% C, 23.42 at.% Al and 37.72 at.% Si. Further analyzed by the red line, the distribution of Si in the pores of the alloy tends to be closer to the carbon element, whereas the Al and B elements were closer to the central region. The XRD patterns of the AlSiB-C/C composites are shown in Figure 5. In addition to the diffraction peaks of the C, Al and Si phases, the SiC, SiB₄ and AlB₁₀ phases were detected. Eustathopoulos et al. [22] and Tong et al. [23] previously showed that SiC could be formed by the reaction between C and liquid Si during infiltration, which is beneficial for wetting and spontaneous infiltration. Moreover, mesophases, including SiB₄ and AlB₁₀, could be produced from molten alloys during cooling. The SiB₄ can hinder the diffusion of oxygen and further protect the carbon fibers [24].

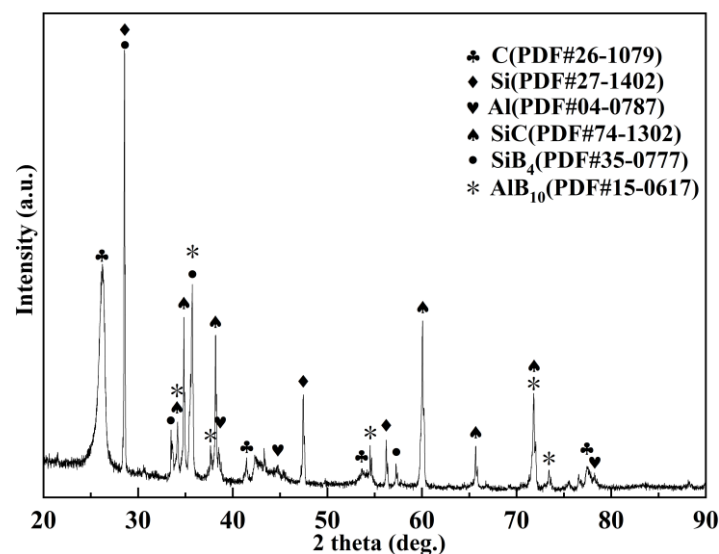


Figure 5. XRD patterns of the AlSiB-C/C composites before ablation.

3.2. Surface Temperature and Ablation Morphology Evolution

Figure 6a shows the surface temperature versus time curve of the oxy-acetylene test for C/C and AlSiB-C/C composite specimens. It is obvious that the temperature curves of the C/C and AlSiB-C/C composites contain two stages, namely the heating stage (Stage 1) and

the constant temperature stage (Stage 2). During the heating stage, it took 55 s for the surface temperature of the C/C composite specimens to rise from room temperature to 1938 °C, whereas it took 25 s for the AlSiB-C/C composite specimens to rise from room temperature to 1697 °C. This is because, in the initial stage of heating, the flame temperature is much higher than the material surface temperature, and at the same time, the thermal diffusivity of AlSiB-C/C composites is higher than that of C/C composites (Figure 6b). Higher thermal diffusivity means that there is a faster heating rate. As a result, the AlSiB-C/C composite specimens reached the constant temperature stage more quickly. After adding the AlSiB alloy, the heat capacity per unit volume increased (Figure 6c), and the AlSiB-C/C composite specimens had higher thermal conductivity (Figure 6d). High thermal conductivity means that there is faster heat transfer from the surface to the interior, which results in a lower surface temperature for the AlSiB-C/C composite compared to the C/C composite. The surfaces of the C/C composite material specimens and the AlSiB-C/C composite material specimens were heated to 1957 °C and 1739 °C within 100 s, respectively. The results show that the addition of the AlSiB alloy effectively reduced the surface temperature at the constant temperature stage. A reduction in the surface temperature of the AlSiB-C/C composites can effectively reduce the thermochemical ablation of C/C composites. After 100 s (Stage 3), the surface temperature of the AlSiB-C/C composite rises slowly because AlSiB alloy is gradually consumed.

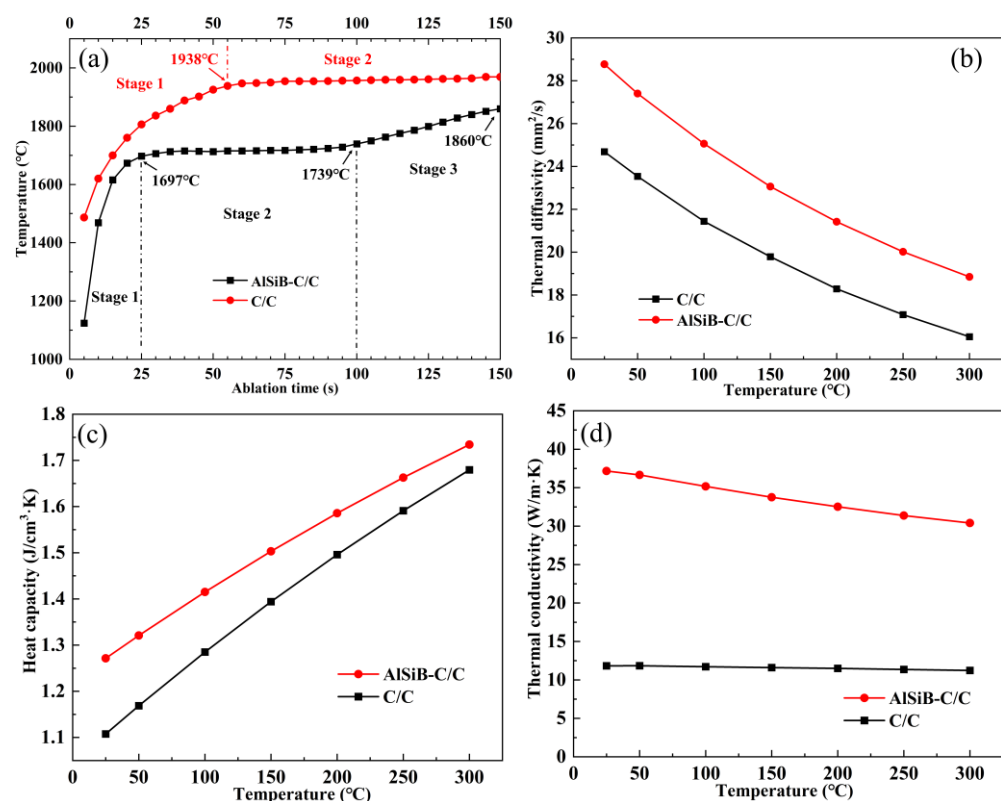


Figure 6. (a) Surface temperature changes during ablation, (b) thermal diffusivity, (c) heat capacity per unit volume and (d) thermal conductivity for the C/C and the AlSiB-C/C composites.

Figure 7 shows the macro-morphologies of the AlSiB-C/C composite specimens ablated for 25 s, 50 s, 100 s and 150 s. As shown in Figure 7a, an inconspicuous ablation pit formed and no damaged carbon fibers were found on the surface at the ablation center of the AlSiB-C/C composite specimens after ablation for 25 s. Meanwhile, as shown in Figure 8a, a lot of molten alloy and pores adhered to the surface, which verifies that the AlSiB alloy melts and overflows during the ablation process. These molten materials were generated by the pressure gradient between the composites inside and the ablation environment, which would create a recoil pressure that forced the molten alloy to gush out from pores in

C/C composites [25,26]. The majority of molten alloy would accumulate and flow, slightly expand, and cover the exposed specimen surface. The AlSiB-C/C composites that are covered by intact, high melting point and high boiling point multilayer oxides are free from denudation. In the first 25 s, the linear ablation rate of the AlSiB-C/C composites specimens is low (about $4.04 \mu\text{m/s}$). This can be explained by the ablation behavior of specimens, which were covered by a dense and successive deposited layer. The molten AlSiB alloy partially evaporates when exposed to the flame, which also causes the consumption of the AlSiB alloy and heat on the surface. AlSiB alloy vapors and gaseous oxidation products (CO , SiO_2 , Al_2O_3 , B_2O_3 etc.) combine to form a gas heat barrier that slows convective heat transfer, which is called the thermal blockage effect [20,25]. These gas oxidation products form bubbles when they discharge from the surface of the composite. The broken bubbles left regular holes on the surface (Figure 8a). From 25 s to 100 s, the dissipative agent in the AlSiB-C/C composite specimens was continuously supplemented to the surface. Although there was still molten material flowing out, a small amount of carbon fiber was exposed. Moreover, as shown in Figure 8b,c, the exposed carbon fibers were distributed parallel to the surface of the specimens, indicating that the molten parallel to the carbon fibers was consumed first. The heat absorbed by these reactions, including melting, evaporation and thermochemical reactions, is in equilibrium with the heat released by the flame heating, resulting in a relatively constant surface temperature of the specimens. Meanwhile, the ablation pits in the central area were also expanding, as shown in Figure 7b,c. Finally, as shown in Figure 8d, at 150 s, the specimen surface was almost not covered by the molten alloy. A large number of carbon fibers were directly exposed to the ablation environment, resulting in a sharp increase in ablation shrinkage and a rise in surface temperature. Table 2 shows that R_l increased with ablation time. As for the AlSiB-C/C composites, the molten alloy melts and evaporates to absorb heat in the first 25 s, which reduces the accumulation of heat and slows down the rise in temperature. The ablation products (Al_2O_3 and SiO_2) form an oxide protective film, which isolates oxygen and hinders further ablation to the inside. When the ablation lasted for 50 s, all the Al in the alloy was consumed. Part of the Al was melted and washed away from the surface of the composites by the airflow, and the other part was converted into Al_2O_3 . An increase in temperature resulted in a decrease in the viscosity of the oxide film and an increase in oxygen permeability. The scouring of the airflow makes it impossible to form a continuous oxide film. The flame acted directly on the surface of the substrate, resulting in an increased rate of linear ablation. As the ablation proceeded, the Si in the alloy was completely consumed. A large number of carbon fibers were directly exposed to the ablative environment, resulting in a significant increase in the rate of linear ablation. In contrast, both the carbon fibers and the carbon matrix in the C/C composite were exposed to the ablative environment within 150 s. High-temperature heat flow and gas scour led to a sharp increase in the rate of linear ablation.

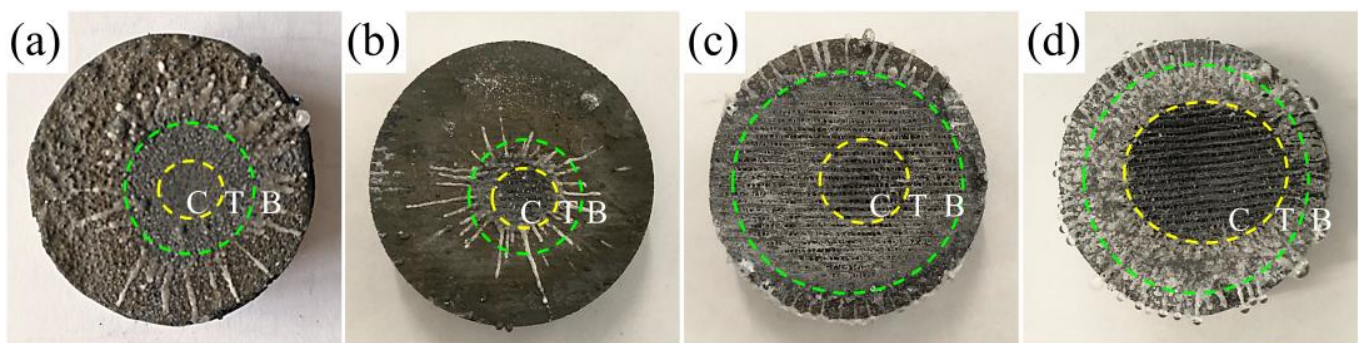


Figure 7. Photographs of the AlSiB-C/C composites after ablating for (a) 25 s, (b) 50 s, (c) 100 s and (d) 150 s (C, center region; T, transition region; B, brim region).

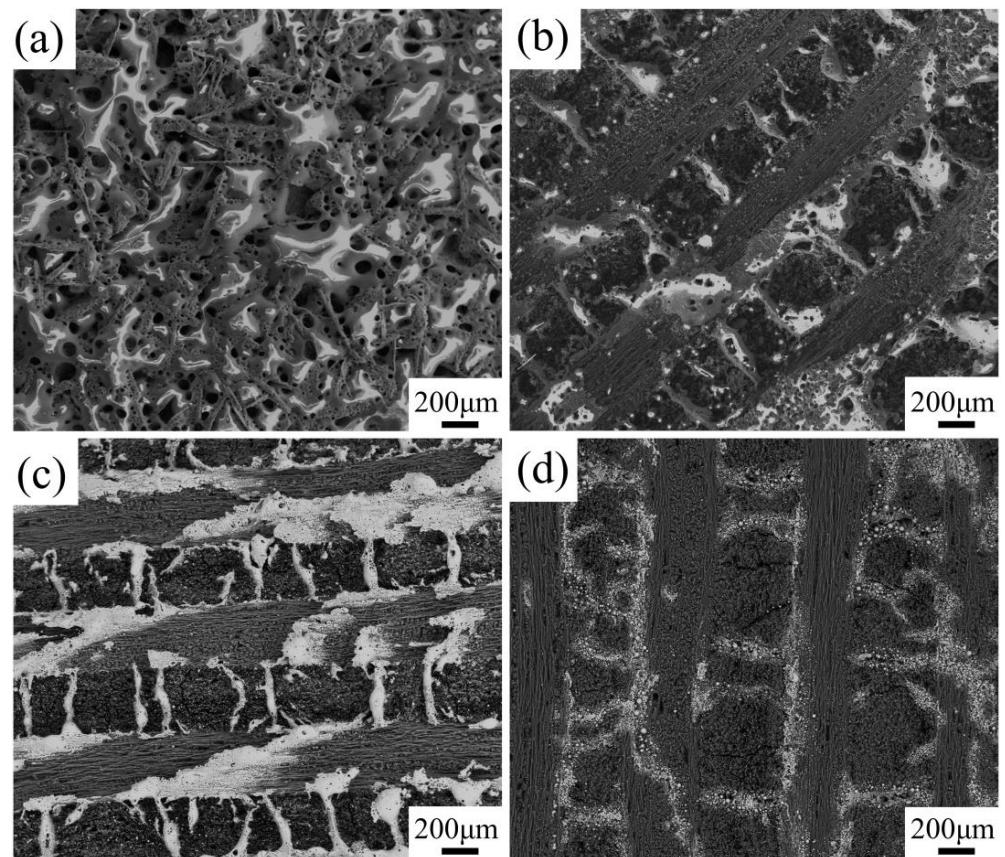
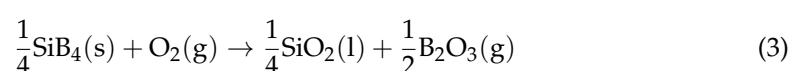


Figure 8. Surface micrographs of the central region of the AlSiB-C/C composites ablated for (a) 25 s, (b) 50 s, (c) 100 s and (d) 150 s.

Table 2. Ablation properties of the composites.

Materials	Surface Temperature Variation of the Ablation Centre/°C				Linear Ablation Rate/ $\times 10^{-3} \text{ mm} \cdot \text{s}^{-1}$			
	25 s	50 s	100 s	150 s	25 s	50 s	100 s	150 s
AlSiB-C/C	1697	1713	1739	1860	4.04	17.68	29.32	47.84
C/C	1806	1925	1957	1969	10.06	27.13	78.26	139.62

The XRD patterns of the central area of the specimens after ablation for 25 s, 50 s, 100 s and 150 s are shown in Figure 9. The composition of the specimens before AlSiB-C/C ablation included C, Al, Si, SiC, AlB₁₀ and SiB₄. Al₂O₃ and SiO₂ were detected 25 s after ablation. This is because Al and Si react with oxygen at high temperatures in order to generate Al₂O₃ and SiO₂. However, AlB₁₀ could be ablated and further converted to Al₂O₃ and B₂O₃. Because the boiling point of B₂O₃ is low, it evaporates easily. As such, B₂O₃ was not detected by XRD. According to these results, it can be inferred that the white glassy substance on the specimen surface shown in Figure 7a is mainly composed of a molten alloy and its oxidation products. When the ablation time was increased to 50 s, Al and AlB₁₀ were all converted to Al₂O₃ (Figure 9b). When the ablation time was increased to 100 s, Si continuously precipitated out. Furthermore, part of the remaining Si reacted with the matrix to form SiC and the other part was directly oxidized to SiO₂ (Figure 9c). At this time, the ablation products had not changed. As the ablation time increased to 150 s, all the Si in the central area was consumed (Figure 9d). At this time, the ablation products were mainly SiC, Al₂O₃ and SiO₂. From 0 to 150 s, with the extension of ablation time, the main chemical reactions were as follows:



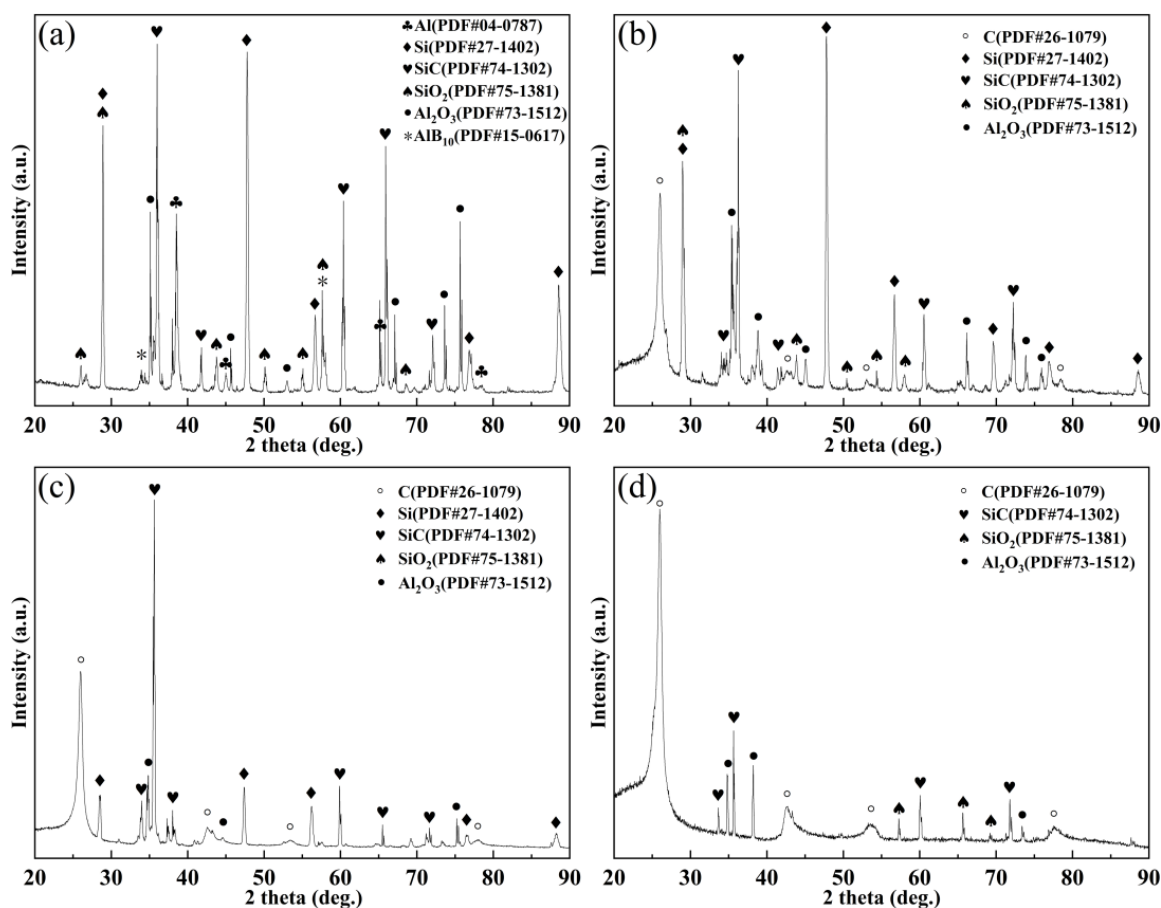
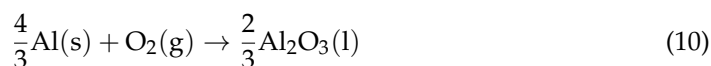
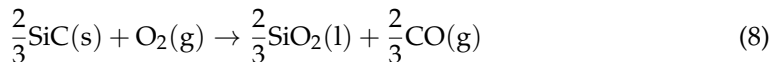
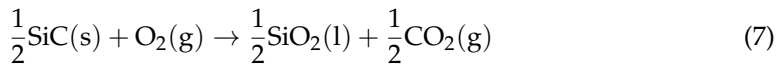
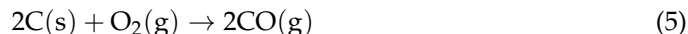
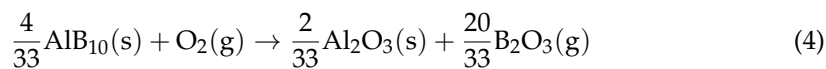


Figure 9. XRD patterns of the central region of the AlSiB-C/C composites ablated for (a) 25 s, (b) 50 s, (c) 100 s and (d) 150 s.

The Gibbs free energy changes (ΔG) in the reactions between C, Al, Si, SiC and O₂ are shown in Figure 10. These oxidation reactions may occur in the temperature range of 0–2500 °C. The smaller the ΔG , the greater the tendency for a chemical reaction.

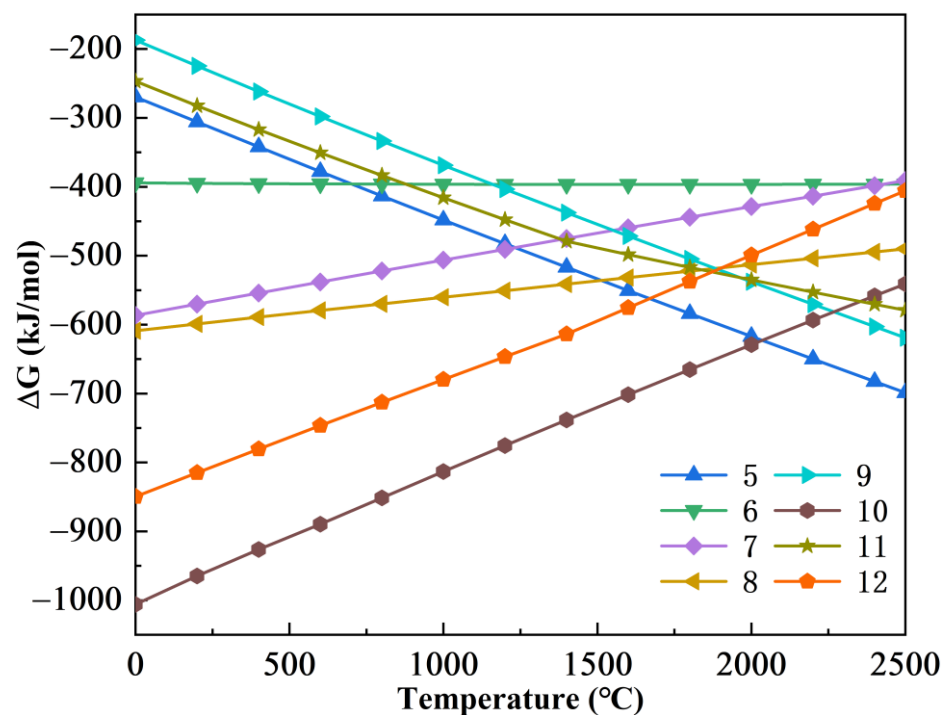


Figure 10. Gibbs free energy change (ΔG) versus the temperature curves.

At the surface temperature of the specimens, Al, Si and SiC mainly undergo passive oxidation (reactions (8), (10) and (12)), resulting in the formation of Al_2O_3 and SiO_2 glassy protective layers [27]. The protective layer has the ability to weaken the oxygen acetylene flow and protect the matrix from ablation. Gas reaction products, such as CO, CO_2 , SiO and B_2O_3 , escape from the surface layer to leave pores, which is unfavorable for forming a continuous protective film. In particular, among the above chemical reactions, the ΔG of reaction (10) is the smallest, followed by reaction (12), indicating that Al and Si preferentially undergo oxidation reactions and cover the specimen surface through air flow diffusion to form a dense oxide film. At the same time, it should be noted that the flame temperature is above 2800 °C, the melting points of Al and Si are 660 °C and 1414 °C, respectively, and the boiling points of Al and Si are 2467 °C and 2844 °C, respectively. As such, the melting and evaporation of the alloy can consume heat and further slow down the rise in temperature. The Gibbs free energy of oxidation to melts (reactions 10 and 12) is more favorable than that of oxidation to gas (reactions 5 and 6), demonstrating that Al and Si preferentially undergo oxidation reactions into melts that cover the specimen surface in order to protect the C/C substrates (Figure 10). As the ablation time continued, Al was consumed first. Part of the Si reacted with C at the interface to generate SiC, and part of it was oxidized to generate SiO_2 . When the surface temperature was low, Al_2O_3 and SiO_2 had high viscosity, which can form a dense protective film to isolate oxygen and protect the matrix from oxidation. The alloy inside the specimens continuously precipitated outward to supplement the consumption of Al_2O_3 and SiO_2 (splash and evaporation) so that the composite maintained a low linear ablation rate.

In general, compared with C/C composites, AlSiB-C/C composites have excellent short-term ablation properties, a short preparation period and a low cost. These preliminary results show that AlSiB-C/C composites have broad application prospects in short-term ablative components, such as small solid rocket motor nozzles.

4. Conclusions

In this work, AlSiB-C/C composites were successfully prepared by RMI processes. The microstructural investigations revealed that the AlSiB alloy filled the interbundle pores and channels in the preform, and that the composite material structure was dense. The

ablation resistance was evaluated using oxy-acetylene ablation testing. The ablation behavior and anti-ablation mechanisms of the AlSiB-C/C composites were analyzed through the evolution of morphology and the linear ablation rate at 25 s, 50 s, 100 s and 150 s. The analyzed results indicated that the linear ablation rate of the AlSiB-C/C composites was only 4.04 $\mu\text{m/s}$ after ablation for 25 s, which was about 60% lower than that of the C/C composites. This was due to the oxide protective film in the ablation product. After ablation for 50 s, the Al in the alloy was depleted. The ablation pit in the central area expanded and the linear ablation rate increased. At this time, the melting and evaporation of Si reduced the surface temperature and supplemented the consumption of surface SiO_2 . In the first 100 s, the surface temperature was significantly reduced by heat dissipation with transpiration cooling of the AlSiB alloy.

Author Contributions: Conceptualization, P.K.; methodology, G.W.; validation, Z.S. and Z.X.; formal analysis, Q.H. and L.C.; investigation, J.S. and H.G.; data curation, P.W., writing—original draft preparation, Q.H. and P.W.; writing—review and editing, Z.W.; project administration, P.K. All authors have read and agreed to the published version of the manuscript.

Funding: This work was supported by the National Natural Science Foundation of China (Grant Numbers: 52273286).

Data Availability Statement: The data presented in this study are available on request from the corresponding author.

Conflicts of Interest: The authors declare no conflict of interest.

References

1. Fitzer, E.; Manocha, L.M. *Carbon Reinforcements and Carbon/Carbon Composites*; Springer Science & Business Media: Berlin, Germany, 1998.
2. Fu, Q.; Zhang, P.; Zhuang, L.; Zhou, L.; Zhang, J.; Wang, J.; Hou, X.; Riedel, R.; Li, H. Micro/nano multiscale reinforcing strategies toward extreme high-temperature applications: Take carbon/carbon composites and their coatings as the examples. *J. Mater. Sci. Technol.* **2022**, *96*, 31–68. [\[CrossRef\]](#)
3. Vignoles, G.L.; Aspa, Y.; Quintard, M. Modelling of carbon–carbon composite ablation in rocket nozzles. *Compos. Sci. Technol.* **2010**, *70*, 1303–1311. [\[CrossRef\]](#)
4. Zhang, Y.; Liu, N.; Chen, L.; Wang, S.; Liu, Y. Determination of the physical properties of functional gradient materials. *J. Solid Rocket. Technol.* **2004**, *27*, 77–80.
5. Fu, Q.; Shan, Y.; Wen, S.; Li, H.; Chu, Y.; Liu, X. Oxidation pre-treatment to improve the mechanical property and oxidation resistance of Si–Mo–Cr coated C/C composites. *Corros. Sci.* **2014**, *83*, 103–110. [\[CrossRef\]](#)
6. Zhou, K.; Xu, J.; Xiao, G.; Huang, Y. A novel low-damage and low-abrasive wear processing method of Cf/SiC ceramic matrix composites: Laser-induced ablation-assisted grinding. *J. Mater. Proc. Technol.* **2022**, *302*, 117503. [\[CrossRef\]](#)
7. Yan, C.; Liu, R.; Zhang, C.; Cao, Y. Ablation and mechanical properties of 3D braided C/ZrC–SiC composites with various SiC/ZrC ratios. *Ceram. Int.* **2016**, *42*, 19019–19026. [\[CrossRef\]](#)
8. Sun, H.; Li, H.; Shen, X.; Cao, G.; Qiang, X.; Ren, X.; Fu, Q. Microstructure and Ablation Behavior of C/C Composites Doped with ZrB₂. *J. Inorg. Mater.* **2011**, *26*, 669–672. [\[CrossRef\]](#)
9. Li, H.; Wang, Y.; Fu, Q.; Chu, Y. SiC Nanowires Toughed HfC Ablative Coating for C/C Composites. *J. Mater. Sci. Technol.* **2015**, *31*, 70–76. [\[CrossRef\]](#)
10. Pu, H.; Niu, Y.; Hu, C.; Wang, G.; Li, H.; Zeng, Y.; Zheng, X. Ablation of vacuum plasma sprayed TaC-based composite coatings. *Ceram. Int.* **2015**, *41*, 11387–11395. [\[CrossRef\]](#)
11. Xu, Z.; Fu, Q.; Liu, L.; Li, H.; Wang, Y.; Yao, X.; He, Z. ZrB₂–SiC coating to protect carbon/carbon composites against ablation. *Surf. Coat. Technol.* **2013**, *226*, 17–21. [\[CrossRef\]](#)
12. Yang, X.; Hu, X.; Su, Z.; Shi, A.; Weng, Y.; Huang, Q. Effect of fiber-oriented direction on mechanical and ablative performance of C/C–HfC–ZrC–SiC composites. *J. Asian Ceram. Soc.* **2020**, *8*, 1162–1174. [\[CrossRef\]](#)
13. Borji, S.; Ahangarkani, M.; Zangeneh-Madar, K.; Valefi, Z. The effect of sintering activator on the erosion behavior of infiltrated W-10wt%Cu composite. *Int. J. Refract. Met. Hard Mater.* **2017**, *66*, 150–157. [\[CrossRef\]](#)
14. Ran, L.; Peng, K.; Yi, M.; Yang, L. Ablation property of a C/C–Cu composite prepared by pressureless infiltration. *Mater. Lett.* **2011**, *65*, 2076–2078. [\[CrossRef\]](#)
15. Zhang, X.; Han, J.; He, X.; Yan, C.; Wang, B.; Xu, Q. Ablation-resistance of combustion synthesized TiB₂–Cu cermet. *J. Am. Ceram. Soc.* **2005**, *88*, 89–94. [\[CrossRef\]](#)
16. Handbook of Practical Inorganic Thermodynamic Data. *Nonferrous Met.* **1980**, *3*, 45.
17. Wu, L.; Wu, G.; Li, B.; Kang, P.; Chen, S.; Yang, W. Ablation behaviour of interpenetrating Al/graphite composites. *Optoelectron. Adv. Mater. -Rapid Commun.* **2015**, *9*, 381–383. [\[CrossRef\]](#)

18. Liu, H.; Kang, P.; Wu, G.; Wang, Z.; Zhang, N.; Mula, S. Ablation mechanism of AlSi/graphite dissipative heat protective composites under an oxy-acetylene torch. *Ceram. Int.* **2021**, *47*, 27925–27933. [[CrossRef](#)]
19. Kang, P.; Liu, H.; Yang, W.; Wang, W.; Zhang, N.; Zhao, Q.; Mula, S.; Wu, G. Microstructure and ablation behavior of SiMo/graphite composites with excellent short-time ablation resistance. *Corros. Sci.* **2020**, *168*, 108590. [[CrossRef](#)]
20. Tian, T.; Sun, W.; Qing, X.; Xiong, X.; Zhang, H.; Chu, Y.; Chen, Z.; Zeng, Y. Intelligent cooling structure design of “Z-pins like” silicon rods to enhance the ablation resistance of C/C-ZrC-SiC composites above 2500 °C. *J. Eur. Ceram. Soc.* **2020**, *40*, 3875–3886. [[CrossRef](#)]
21. Liu, Y.; Fu, Q.; Wang, B.; Liu, T.; Sun, J. The ablation behavior and mechanical property of C/C-SiC-ZrB₂ composites fabricated by reactive melt infiltration. *Ceram. Int.* **2017**, *43*, 6138–6147. [[CrossRef](#)]
22. Eustathopoulos, N.; Israel, R.; Drevet, B.; Camel, D. Reactive infiltration by Si: Infiltration versus wetting. *Scr. Mater.* **2010**, *62*, 966–971. [[CrossRef](#)]
23. Tong, Y.; Bai, S.; Liang, X.; Qin, Q.H.; Zhai, J. Reactive melt infiltration fabrication of C/C-SiC composite: Wetting and infiltration. *Ceram. Int.* **2016**, *42*, 17174–17178. [[CrossRef](#)]
24. Shi, F.; Yin, X.; Fan, X.; Cheng, L.; Zhang, L. A new route to fabricate SiB₄ modified C/SiC composites. *J. Eur. Ceram. Soc.* **2010**, *30*, 1955–1962. [[CrossRef](#)]
25. Li, B.; Kang, P.; Gou, H.; Wu, G.; Mula, S. Surface morphology evolution and ablation mechanism of SiC-Si multiphase ceramic coating on graphite under oxy-acetylene flame. *Corros. Sci.* **2014**, *88*, 473–480. [[CrossRef](#)]
26. Jia, J.; Bai, S.; Xiong, D.; Chen, Q.; Li, C.; Gao, M. Microstructure and ablation behaviour of a Cf/SiC-Al composite prepared by infiltrating Al alloy into Cf/SiC. *J. Alloys Compd.* **2022**, *895*, 162430. [[CrossRef](#)]
27. Huo, C.; Guo, L.; Zhou, L.; Liu, B.; Wang, C.; Zhang, Y.; Wang, H. Effect of Al₂O₃ addition on the ablation behavior of SiC-ZrC coated C/C composites. *J. Alloys Compd.* **2018**, *752*, 489–504. [[CrossRef](#)]

Disclaimer/Publisher’s Note: The statements, opinions and data contained in all publications are solely those of the individual author(s) and contributor(s) and not of MDPI and/or the editor(s). MDPI and/or the editor(s) disclaim responsibility for any injury to people or property resulting from any ideas, methods, instructions or products referred to in the content.